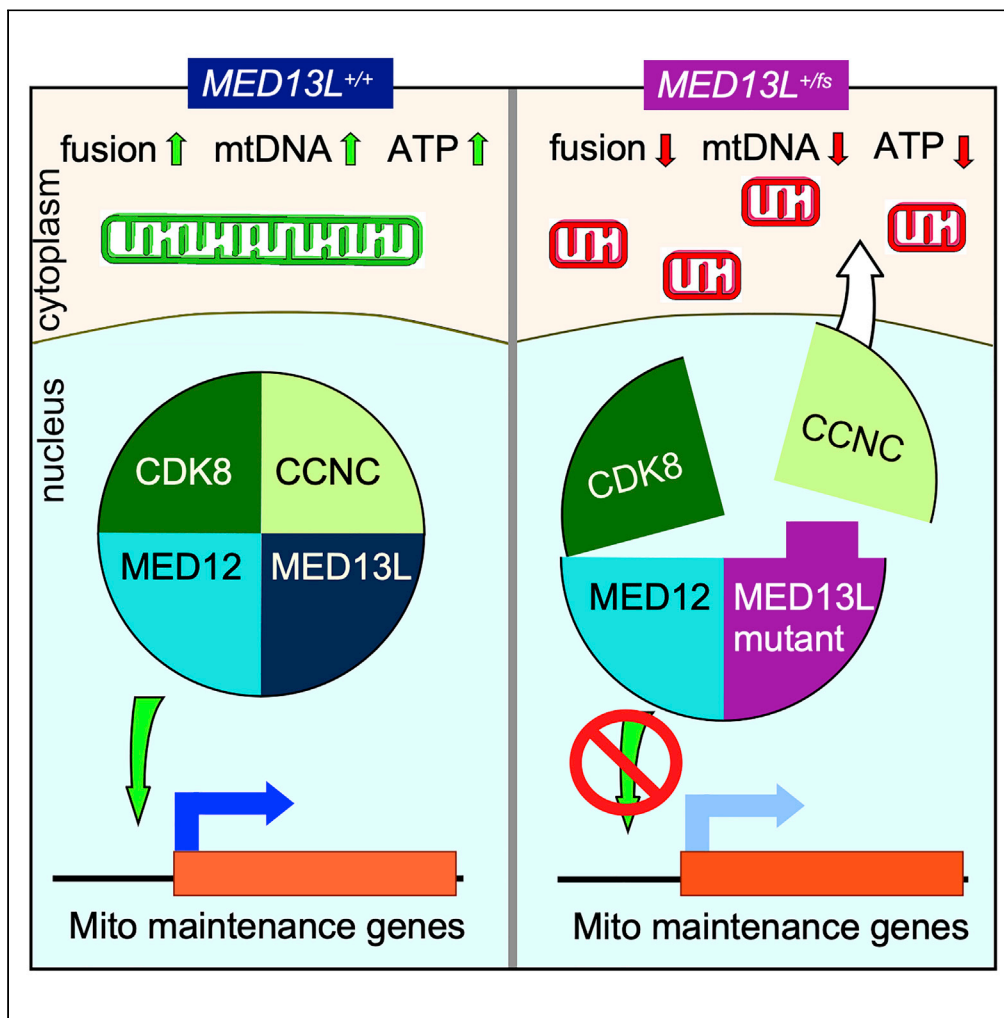


Article

Aberrant cyclin C nuclear release induces mitochondrial fragmentation and dysfunction in *MED13L* syndrome fibroblasts



Kai-Ti Chang, Jan Jezek, Alicia N. Campbell, ..., Warren D. Kruger, Peter M. van Hasselt, Randy Strich

strichra@rowan.edu

Highlights
MED13L haplo-insufficiency mutation causes aberrant cyclin C nuclear release

Cyclin C nuclear release fragments mitochondria and increases endogenous ROS

MED13L syndrome patient fibroblasts exhibit reduced mitochondrial function

MED13L syndrome patient fibroblasts exhibit reduced mtDNA copy number

Chang et al., iScience 25, 103823
 February 18, 2022 © 2022 The Author(s).
<https://doi.org/10.1016/j.isci.2022.103823>



Article

Aberrant cyclin C nuclear release induces mitochondrial fragmentation and dysfunction in *MED13L* syndrome fibroblasts

Kai-Ti Chang,^{1,5} Jan Jezek,^{1,6} Alicia N. Campbell,¹ David C. Stieg,¹ Zachary A. Kiss,² Kevin Kemper,¹ Ping Jiang,¹ Hyung-Ok Lee,³ Warren D. Kruger,³ Peter M. van Hasselt,⁴ and Randy Strich^{1,7,*}

SUMMARY

***MED13L* syndrome is a haploinsufficiency developmental disorder characterized by intellectual disability, heart malformation, and hypotonia. *MED13L* controls transcription by tethering the cyclin C-Cdk8 kinase module (CKM) to the Mediator complex. In addition, cyclin C has CKM-independent roles in the cytoplasm directing stress-induced mitochondrial fragmentation and regulated cell death. Unstressed *MED13L*^{S1497F/fs} patient fibroblasts exhibited aberrant cytoplasmic cyclin C localization, mitochondrial fragmentation, and a 6-fold reduction in respiration. In addition, the fibroblasts exhibited reduced mtDNA copy number, reduction in mitochondrial membrane integrity, and hypersensitivity to oxidative stress. Finally, transcriptional analysis of *MED13L* mutant fibroblasts revealed reduced mRNA levels for several genes necessary for normal mitochondrial function. Pharmacological or genetic approaches preventing cyclin C-mitochondrial localization corrected the fragmented mitochondrial phenotype and partially restored organelle function. In conclusion, this study found that mitochondrial dysfunction is an underlying defect in cells harboring the *MED13L*^{S1497F/fs} allele and identified cyclin C mis-localization as the likely cause. These results provide a new avenue for understanding this disorder.**

INTRODUCTION

MED13L syndrome is an autosomal dominant spectrum disorder diagnosed in children that is denoted by several features including moderate intellectual disability (ID), speech impairment, dysmorphic facial features, heart malformation, and muscle hypotonia (Torrington et al., 2019). Typical of these disorders, not all patients present with the same scope or severity of symptoms (Adegbola et al., 2015; Asadollahi et al., 2017; Snijders Blok et al., 2018; van Haelst et al., 2015). In the study of over 1000 patients with undiagnosed developmental disorders, 0.5%–1% exhibited *de novo* *MED13L* loss of function mutations (Deciphering Developmental Disorders, 2015). These findings suggest that *MED13L* mutation is a major factor in ID presentation. Although several *MED13L* mutations have been associated with this syndrome, a causative mechanism(s) for the multiple facets of this disorder has not been established.

CCNC (cyclin C), and one each of the CDK8/CDK19, MED12/MED12L, and MED13/MED13L paralogs, form the CDK8 kinase module (CKM), a highly conserved subcomplex of the RNA polymerase II Mediator (Bourbon, 2008). Transcriptome results revealed that cyclin C plays both a positive and negative role in transcription with many genes involved in the stress response and energetics (Li et al., 2014; Stieg et al., 2019). In addition to its transcriptional role, cyclin C also has a cytoplasmic function in stressed cells (Jezek et al., 2019b; Wang et al., 2015). Specifically, exposure to several stressors induces partial cyclin C nuclear release which in turn directly stimulates both stress-induced mitochondrial fission (Cooper et al., 2014; Ganesan et al., 2019) and intrinsic regulated cell death (iRCD) (Jezek et al., 2019a; Wang et al., 2015). Importantly, cytoplasmic cyclin C is sufficient to induce mitochondrial fission but not iRCD in the absence of additional stress (Jezek et al., 2019a; Wang et al., 2015) although it does make cells hypersensitive to oxidative damage (Jezek et al., 2019b).

Several results indicate that MED13 or MED13L anchors cyclin C in the nucleus. First, structural and genetic studies revealed that MED13 or MED13L tethers the CKM to the Mediator in mammalian cells (Hoepfner

¹Department of Molecular Biology, Graduate School of Biomedical Sciences, Rowan University School of Osteopathic Medicine, Stratford, NJ 08084, USA

²Department of Medicine, Rowan University School of Osteopathic Medicine, Stratford, NJ 08084, USA

³Fox Chase Cancer Center, Philadelphia, PA 19111, USA

⁴Department of Metabolic and Endocrine Disease, University of Utrecht Medical Center, Utrecht, 3584 CX, the Netherlands

⁵Present address: Euproprotein Inc., North Brunswick Township, NJ 08989, USA

⁶Present address: The Gurdon Inst., University of Cambridge, CB1 0DF, UK

⁷Lead contact

*Correspondence:

strichra@rowan.edu

<https://doi.org/10.1016/j.isci.2022.103823>



et al., 2005; Li et al., 2021). In addition, cyclin C-CDK8 promoter retention in unstressed cells is directly tied to MED13 turnover (Davis et al., 2013). Genetic analyses in yeast revealed that deleting *MED13* results in partial cyclin C nuclear release (Khakhina et al., 2014). Moreover, preventing Med13 destruction in stressed yeast cells results in cyclin C nuclear retention (Stieg et al., 2018). Finally, constitutively cytoplasmic yeast cyclin C not only results in continuously fragmented mitochondria but also in a loss of mitochondrial function (Khakhina et al., 2014). Taken together, these studies point to a conserved role for MED13 and MED13L in anchoring cyclin C in the nucleus. In addition, these findings also suggest that long-term mitochondrial scission induced by constitutive cytoplasmic cyclin C is detrimental to organelle function. This report describes aberrant cyclin C subcellular location in *MED13L* syndrome patient fibroblasts and the impact this defect has on mitochondrial homeostasis and sensitivity to oxidative stress.

RESULTS

Cyclin C exhibits aberrant cytoplasmic localization in unstressed *MED13L*^{S1497 F/fs} fibroblasts

A six-year-old male patient presenting with heart malformation, ID, and hypotonia was further examined using whole exome sequencing of genomic DNA extracted from a peripheral blood sample. These results revealed a thymidine duplication NM_015335.5:c.[5054dupT]; [(Ser1497Phe/fs)] in exon20 of *MED13L*. This duplication resulted in a frameshift mutation (*MED13L*^{S1497 F/fs}) truncating the protein in exon21. Given the conserved role of MED13/MED13L in retaining cyclin C in the nucleus, immunofluorescence was used to monitor cyclin C localization and mitochondrial morphology in mortal skin fibroblasts isolated from the patient. As expected, cyclin C was primarily nuclear and the mitochondria exhibited long, interconnected tubules in the control WI-38 human lung fibroblasts (top row, Figure 1A). However, the *MED13L*^{+/S1497 F/fs} (denoted *MED13L*^{+fs} for simplicity) cells exhibited elevated cyclin C cytoplasmic localization and extensive mitochondrial fragmentation (third row, Figure 1A). Quantification revealed over 90% of the *MED13L*^{+fs} cells exhibited fragmented mitochondria compared to 20% for the control (boxed numbers, Figure 1A). In addition, these studies revealed co-localization between cytoplasmic cyclin C and mitochondria (Figure 1A, arrows, third row in zoom panel). We previously found that treating cells with the cytoplasmic chaperone inhibitor pifithrin μ (PFT) (Strom et al., 2006) blocked cyclin C-mitochondrial localization (Wang et al., 2015). Treating cells with PFT (1 μ M) partially restored mitochondrial fusion within 24 h (Figure 1A, bottom panels) arguing that cyclin C mis-localization is responsible for mitochondrial fragmentation in *MED13L*^{+fs} cells.

MED13L^{+fs} cells exhibit reduced mitochondrial activity

Previous studies (Hori et al., 2011; Scheibye-Knudsen et al., 2015), including our own in yeast (Khakhina et al., 2014), found that continuous mitochondrial fragmentation is associated with mitochondrial dysfunction. To test mitochondrial output in *MED13L*^{+fs} cells, oxygen consumption was measured via Seahorse metabolic flux analysis. Using WI-38 cultures as a control, we found that *MED13L*^{+fs} cells exhibited a 6-fold reduction in oxygen consumption rate (OCR, Figure 1B) and a 3-fold reduction in respiratory ATP production (Figure 1C). In addition, maximum respiratory activity was also reduced in *MED13L*^{+fs} cells (Figure 1D). These results suggest that mitochondrial respiration is reduced in *MED13L*^{+fs} cells. Support for this conclusion was obtained with the analysis of citric acid cycle and electron transport chain activities in a patient's skeletal muscle tissue biopsy. This study revealed reduced activity in components of both pathways (Table 1) indicating mitochondrial dysfunction in a different tissue type. As these studies were standardized to citrate synthase (CS) activity, one possible explanation is that CS mRNA levels are reduced in the *MED13L*^{+fs} cell line resulting in apparent lower overall activity for many of these assays. To test this possibility, we used RNAseq to measure CS mRNA levels in wild-type (*Ccnc*^{+/+}) or deleted (*Ccnc*^{-/-}) mouse embryonic fibroblasts. The rationale for this study was that deleting *Ccnc* should inactivate all CKM complexes providing a more robust signal. Feature counts of CS mRNA were normalized to *ActB* mRNA levels. These experiments revealed no change in CS transcription in *Ccnc*^{-/-} cells (Figure 1E) indicating that CS levels were not altered and that *MED13L*^{+fs} cells exhibited reduced mitochondrial function.

Our results are consistent with a model that aberrant cyclin C nuclear release results in constitutive mitochondrial fragmentation and organelle dysfunction. To explore this possibility further, mitochondrial activity was measured in *MED13L*^{+fs} cells following PFT treatment (1 μ M, 96 h). Although no significant change in activity was observed with WI-38 control, the *MED13L*^{+fs} cells exhibited increased OCR, respiratory ATP synthesis, and respiratory maximum (Figures 1B–1D). We were unable to extend these experiments for a longer duration as PFT treatment proved toxic after prolonged

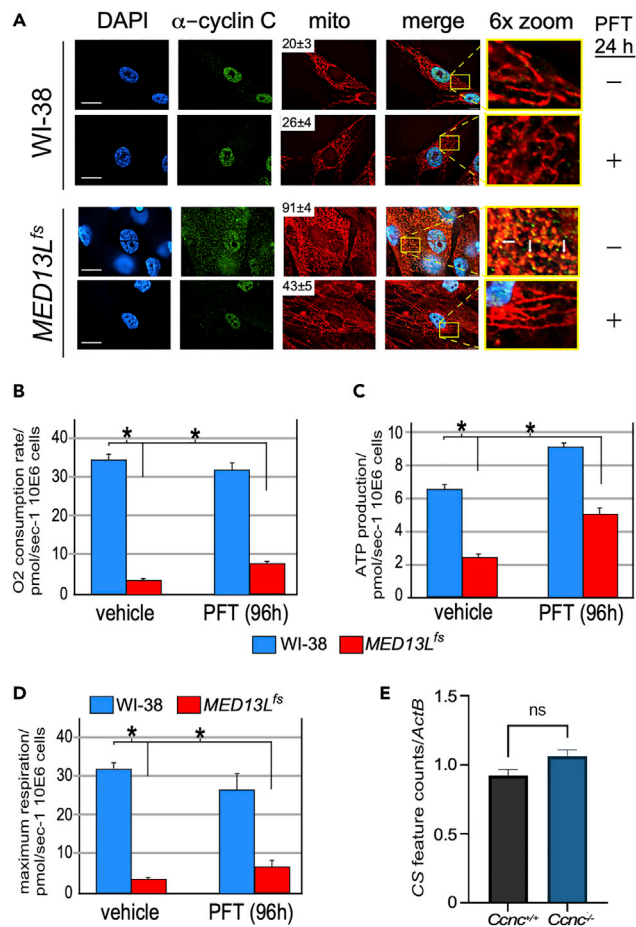


Figure 1. *MED13L*^{+/-} cells exhibit cyclin C nuclear release and mitochondrial dysfunction

(A) The cultures indicated were monitored for nuclear (DAPI), cyclin C (immunohistochemistry), and mitochondrial morphology (MitoTracker). Numbers in mito panels indicate % of population exhibiting fragmented mitochondria (n = 3). Samples treated with PFT (1 μ M, 24 h) are indicated. Arrows indicate cyclin C-mitochondrial co-localization. Bar = 20 μ M, zoom = 6X magnification.

(B–D) (B) Seahorse analysis of the indicated cell lines quantifying basal respiration (B), ATP production (C) and maximum respiration (D) for vehicle and PFT treated (1 μ M, 96 h).

(E) RNA-seq analysis of CS mRNA levels in MEF cultures with the indicated genotypes. Values from three independent cultures were normalized to *ActB*. SEM is shown. *, $p < 0.01$

treatment. However, these results indicate that the mitochondrial hyper-fission phenotype, and to some extent mitochondrial dysfunction, is reversible by preventing cyclin C relocalization to the mitochondria.

Enhanced glycolysis and mitochondrial dysfunction were observed in MEF cells deleted for the fusion factors *Mfn1* and *Mfn2* (Chen et al., 2003, 2010). In addition, mitochondrial dysfunction has been associated with increased glycolytic activity in several pathological states including cancer and vascular disease (Hu et al., 2012). Therefore, we examined glycolytic activity in *MED13L*^{+/-} cells using Seahorse metabolic flux analysis by indirectly measuring lactate production using change in pH. Multiple experiments revealed either no change (trial 1) or increase (trial 2) in glycolytic activity for *MED13L*^{+/-} compared to control WI-38 cultures (Figure S1A). The addition of PFT for 96 h resulted in a slight reduction in glycolysis in for both cell lines. In addition, a modest elevation of serum lactate levels (2.4 mmol/L (normal range 0.5–2.2) was also noted in the patient. Finally, glycolytic activity was measured indirectly by quantifying lactate dehydrogenase A (LDHA) levels (Vander Heiden et al., 2009). Increased glycolysis stimulates LDHA production. Western blot analysis revealed a 1.6-fold increase in LDHA in the *MED13L*^{+/-} cells compared to control

Table 1. Mitochondrial activities in muscle biopsy of patient with *MED13L*^{S1947 F/fs}

Test	Patient values mU CS	Normal range
[1- ¹⁴ C]pyruvate + malate	2.83	3.61–7.48
[1- ¹⁴ C]pyruvate + carnitine	3.68	2.84–8.24
[1- ¹⁴ C]pyruvate + malonate	3.19	3.43–7.3
[U- ¹⁴ C]malate + acetylcarnitine + malonate	2.54	3.43–7.3
[U- ¹⁴ C]malate + acetylcarnitine + arsenite	1.24	2.05–3.85
[1,4- ¹⁴ C]succinate + acetylcarnitine	1.6	2.54–6.39
Reduced ATP + Creatine-phosphate	21	42–81
CI NADH:Q1 Oxydereductase	90 mU/U CS	70–250
CII Succinate Dehydrogenase	77 mU/U CS	67–177
CIII cyt C Oxydereductase	1914 mU/U CS	2200–6610
CIV cyt C Oxydase	1227	810–3120
CII + CIII	214 mU/U CS	300–970

CS, citrate synthase.

(Figure S1B, quantified in Figure S1C) but did not satisfy the significance cutoff. Taken together, these results indicate that mitochondrial function is reduced in *MED13L*^{+fs} cells. In addition, this reduced energy production may be compensated, at least in part, by increased glycolysis.

***MED13L*^{+fs} cells exhibit reduced mtDNA copy number**

The reduction in mitochondrial output can be due to many factors including defects in nuclear transcription of mitochondria-destined proteins, loss of mtDNA integrity, or both. For mtDNA maintenance, mitochondrial dynamics play important roles as fusion is associated with elevated recombination and repair while constitutive mitochondrial fission contributes to nucleoid loss (Chen, 2013). We used a qPCR-based approach to measure mtDNA copy number (Phillips et al., 2014) by comparing the mtMinArc region (Figure S2A) to a genomic locus. These experiments revealed a 2-fold reduction in mtDNA levels in the mutant fibroblasts compared to control (Figure 2A). These findings suggest that reduced mtDNA copy number contributes to the mitochondrial dysfunction observed in *MED13L*^{+fs} cells.

The mtDNA is found in protein-DNA complexes termed nucleoids with each containing 1–15 copies of the mitochondrial genome (Sato and Kuroiwa, 1991). Previous studies have identified several factors involved in nucleoid maintenance including mtDNA binding proteins (Chen and Butow, 2005) and factors controlling mitochondrial shape (Chan, 2020; Youngman et al., 2004). For example, causing constitutive mitochondrial fragmented by deleting the fusion factors *Mfn1* and *Mfn2* resulted in nucleoid loss in individual mitochondrion (Silva Ramos et al., 2019). Using antibodies directed at dsDNA, we calculated the number of nucleoids associated with individual mitochondrion in WI-38 and *MED13L*^{+fs} cells. Because WI-38 contains fused mitochondria with multiple nucleoids (Figure 2C), these cells were treated with H₂O₂ to induce fragmentation. This allowed the number of nucleoids per mitochondrion to be assessed. As expected, nearly all the mitochondria contained nucleoids in treated WI-38 cells (Figure 2C, second row). However, only 57% and 61% of the mitochondria contained nucleoids in untreated and treated *MED13L*^{+fs} cells, respectively. These results indicate that a significant portion of the mitochondria lack detectable nucleoid DNA which correlates with reduced mtDNA copy number and mitochondrial dysfunction.

***MED13L*^{+fs} cells exhibit reduced transcription of nuclear-encoded mitochondrial proteins**

Of the ~1500 proteins that compose the mitochondria, the vast majority are encoded by the nuclear genome (Diaz and Moraes, 2008). We previously described the cyclin C-dependent transcriptome in mice focusing on the oxidative stress response (Stieg et al., 2019). Interrogation of these datasets revealed several genes exhibiting reduced transcription in the *Ccnc*^{-/-} mouse embryonic fibroblast (MEF) cell line that had mitochondrion GO terms (Figure S2B). We tested five genes and found that two genes, *TFB1M* (a mitochondrial transcription specificity factor) and *MDH1* (malate dehydrogenase) exhibited modest reductions in mRNA levels in *MED13L*^{+fs} cells compared to WI-38 controls (Figure 2D).

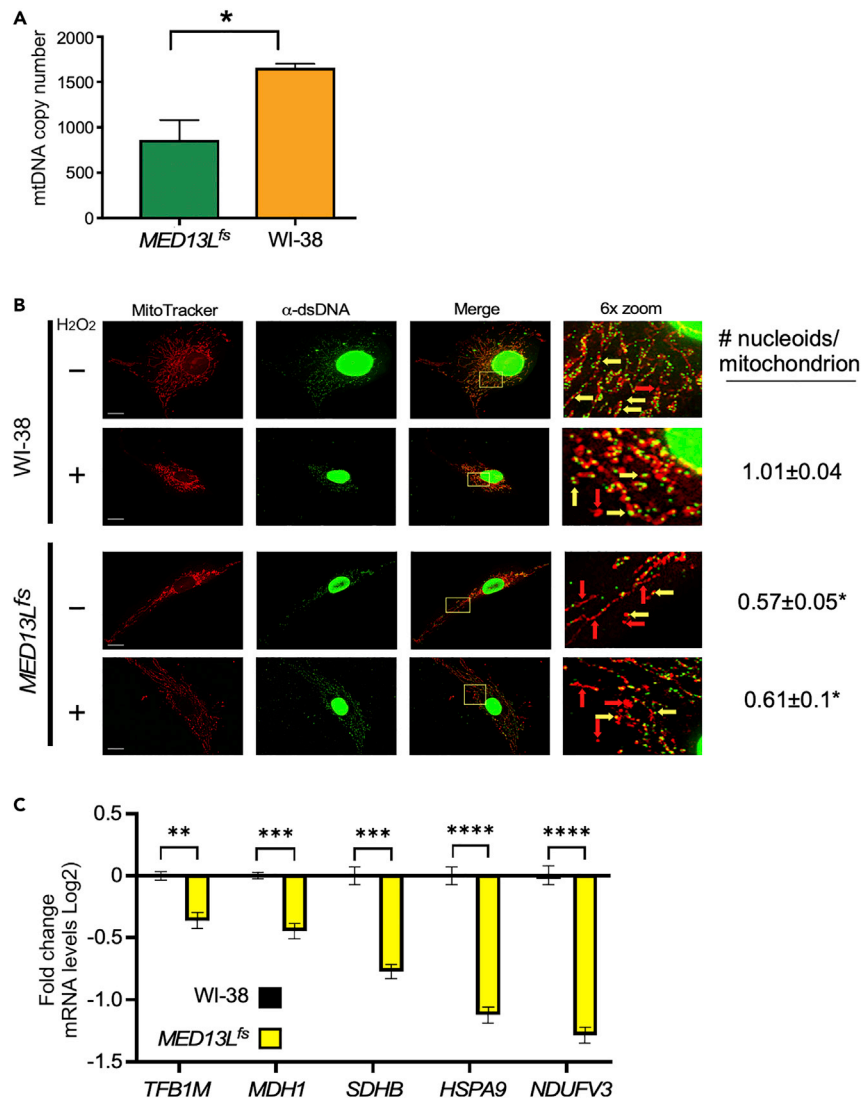


Figure 2. *MED13L^{+/-}* cells exhibit reduced mtDNA copy number, nucleoid retention, and mitochondrial maintenance gene transcription

(A) qPCR results from the minor arc with the indicated human fibroblasts. The $-\Delta\text{CT}$ was calculated with a nuclear gene (*β 2M*) used as the internal control. Error bars indicate SEM (n = 3 biological replicates performed in triplicate).

(B) Visualization of mtDNA nucleoids in WT and *MED13L^{+/-}* cells. Cells were fixed and co-stained with MitoTracker red and α -dsDNA antibodies. Boxed regions in merged images are enlarged in the right panels. Values presented represent the number of nucleoids per individual mitochondrion. Values for untreated WI-38 cells were not included as mitochondria were fused with multiple nucleoids. Asterisks indicate statistical differences from treated WI-38 value. Bar = 20 μ M.

(C) RT-qPCR mRNA quantification of the indicated genes in unstressed *MED13L^{+/-}* and WI-38 cells. Changes in mRNA levels are indicated (\log_2) compared to WI-38 control cells. SEM is shown. * = $p < 0.05$; ** = $p < 0.01$; *** = $p < 0.005$; **** = $p < 0.001$.

Transcript levels of *SDHB* (Succinate Dehydrogenase Complex Iron Sulfur Subunit B) were slightly more suppressed while *HSPA9* (mitochondrial chaperone) and *NDUFV3* (NADH: Ubiquinone Oxidoreductase Subunit V3) were more severely affected. Consistent with this latter finding, ubiquinone oxidoreductase activity was at the lower end of the normal range in the muscle biopsy (Table 1). Therefore, despite the presence of two wild-type copies of *MED13* and one copy of *MED13L*, transcriptional defects in mitochondrial-directed genes were detected in *MED13L^{+/-}* cells. These results suggest that the mitochondrial dysfunction observed in *MED13L^{+/-}* cells are due to both nuclear and mitochondrial-specific defects. The exact contribution of each arm of the mitochondrial maintenance pathway is yet to be established.

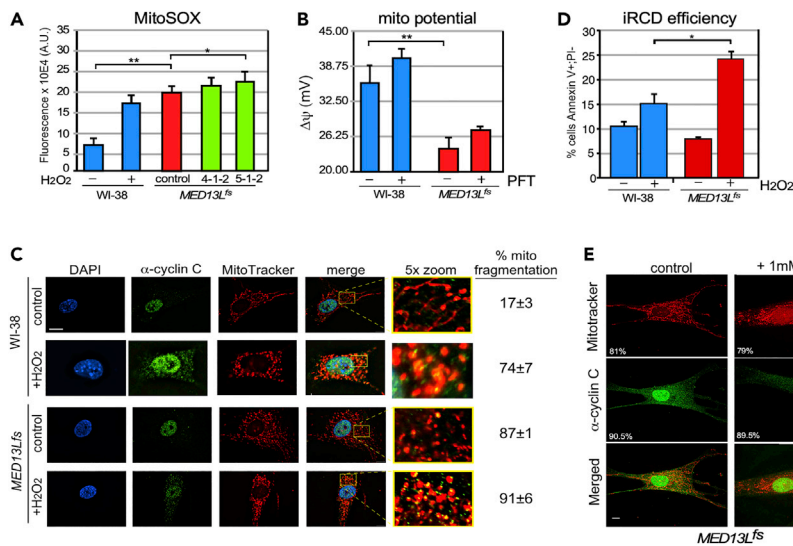


Figure 3. *MED13L*^{+/fs} cells exhibit loss of mitochondrial integrity and enhanced ROS sensitivity

(A) Endogenous mitochondrial ROS was measured in the cells indicated using mitochondrial-specific ROS activated fluorescent dye MitoSOX. H₂O₂-treated WI-38 cells served as a positive control for MitoSOX oxidation. N = 3 for all samples. Means ± SEM are shown.

(B) Mitochondrial membrane potential for the indicated cell lines with or without PFT added (1 μM, 96 h) was calculated using TMRM staining as described in STAR methods.

(C) WI-38 and *MED13L*^{+/fs} cells were treated with H₂O₂ (0.4 mM, 4 h) as indicated and mitochondrial morphology (MitoTracker) and the subcellular localization of the nucleus (DAPI staining) and cyclin C (immunohistochemistry) were determined. The percentages of the population exhibiting fragmented mitochondria are shown on the right.

(D) Intrinsic regulated cell death (iRCD) was measured in the indicated cell lines with or without H₂O₂ addition (0.4 mM, 16 h). The percentages of the populations that were Annexin V positive, propidium iodide negative as determined by FAC analysis are shown. N = 3 for all experiments, means ± SEM are shown. * = p < 0.05; ** = p < 0.01. Bar = 20 μM.

(E) Mitochondrial morphology and cyclin C subcellular localization were determined for *MED13L*^{+/fs} cells with and without NAC treatment as indicated. The percent of cells exhibiting fragmented mitochondria or cytoplasmic cyclin C (>50 cells counted) are indicated in the MitoRed and α-cyclin C panels, respectively. Bar = 10 μM

MED13L^{+/fs} cells exhibit elevated ROS and sensitivity to oxidative stress

Previous studies have reported that cells undergoing extensive mitochondrial fragmentation also exhibit elevated endogenous reactive oxygen species (ROS) levels perhaps due to disrupting the ETC complexes (Hung et al., 2018). To examine this question, *MED13L*^{+/fs} cells were treated with a mitochondrial-specific redox sensor (MitoSOX) followed by fluorescence-activated cell analyses. We found that *MED13L*^{+/fs} cells exhibited a significant elevation in MitoSOX oxidation compared to the WI-38 control (Figure 3A). To further explore the health of the mitochondria, WI-38 and *MED13L*^{+/fs} cells were treated with TMRM, a dye that fluoresces in the oxidative environment of intact mitochondria. These studies found statistically significant reduction in membrane potential ($\Delta\psi$) in *MED13L*^{+/fs} cells (Figure 3B). These findings indicate that the *MED13L*^{+/fs} mutation reduces mitochondrial function and health. Repeating these experiments with PFT treatment for 96 h did not produce a statistically significant recovery of mitochondrial membrane potential although the results were trending in that direction.

Many cell types are sensitive to elevated endogenous ROS including neurons (Calabrese et al., 2005; Li et al., 2013). To test whether the *MED13L*^{fs} allele sensitized the fibroblasts to reactive oxygen, these cells were treated with H₂O₂ and cyclin C subcellular localization, mitochondrial morphology and intrinsic regulated cell death (iRCD, a.k.a. apoptosis) efficiency were monitored. In WI-38 control cells, H₂O₂ treatment induced the anticipated cyclin C release and mitochondrial fragmentation (Figure 3C). In the *MED13L*^{+/fs} cells, cyclin C levels in the cytoplasm were elevated over untreated controls but no quantitative difference in percentage of cells exhibiting mitochondrial fragmentation was observed following H₂O₂ treatment (Figure 3C).

Our previous work indicated that cytoplasmic cyclin C stimulated mitochondrial localization of Bax, a Bcl-2 family member that triggers iRCD (Jezek et al., 2019a). Although cytoplasmic cyclin C did not stimulate

cell death on its own, it did make cells hypersensitive to oxidative stress. To test whether the cytoplasmic cyclin C in *MED13L*^{+/*fs*} cells altered sensitivity to H₂O₂-induced iRCD, two cell death signals, Annexin V reactivity and propidium iodide (PI) permeability were monitored. In these assays, only Annexin V-positive, PI-negative cells were counted to eliminate the contribution from necrotic cells. In the absence of any exogenous stress, the presence of the *MED13L*^{*fs*} allele did not enhance iRCD execution (Figure 3D). However, treatment with low-dose H₂O₂ stimulated a significant increase in iRCD in the *MED13L*^{*fs*} cells compared to the control. These findings indicate that the *MED13L*^{*fs*} allele does not induce cell death on its own but does sensitize fibroblasts to oxidative insults. As cyclin C relocates to the cytoplasm following oxidative stress (Wang et al., 2015), one possible cause of aberrant cyclin C localization in *MED13L*^{+/*fs*} cells is elevated ROS and not disruption of binding to the Mediator. To test this possibility, N-acetyl cysteine (NAC) was added to *MED13L*^{+/*fs*} cells for 2 h; then, cyclin C localization and mitochondrial morphology were accessed. Two hours was chosen as this was sufficient time to blunt the impact of H₂O₂ treatment on cyclin C function (Jezek et al., 2019a). These studies revealed no change in cyclin C localization or mitochondrial fragmentation following NAC treatment (Figure 3E). Taken together, these results indicate that cyclin C cytoplasmic localization is due to the *MED13L*^{*fs*} mutation and that the presence of cyclin C at the mitochondria sensitizes cells to oxidative stress.

Correcting the *MED13L*^{*fs*} mutation restores mitochondrial fusion

As described earlier, PFT treatment partially reversed *MED13L*^{*fs*}-induced mitochondrial hyper-fragmentation indicating that aberrant cyclin C localization to the mitochondria was the basis for organelle fragmentation (Figure 1A). However, as a chaperone inhibitor, it is still possible that the impact of PFT treatment is not solely mediated through cyclin C localization. As described earlier, the *MED13L*^{*fs*} allele possesses an extra thymidine in exon 20 terminating the protein in exon 21 (Figure 4A). To correct this mutation, we used a new CRISPR approach termed *in situ* cut-and-paste (iCAP) that utilizes the Cas9 or Cas12a genome editing enzymes to generate precise double-strand breaks (Figure 4B). Placing the identical nuclease target sites flanking the wild-type sequence on the replacement template (RT) provides a substrate for seamless replacement of the mutant allele. In addition, the RT harbors a puromycin resistance gene to identify transfectants (see Figure 4B for Cas12a example). Following transfection, two antibiotic resistant pools obtained from the Cas9 and Cas12a iCAP procedures (4-1-2 and 5-1-2, respectively) were selected for further study. PCR genotyping and sequencing of iCAP replacement insertions revealed that the mutation in exon 20 was corrected. To determine if correcting the frameshift mutation altered mitochondrial morphology and cyclin C localization, fluorescence microscopy was employed. Compared to the *MED13L*^{+/*fs*} cell line, 4-1-2 and 5-1-2 cell pools exhibited reduced mitochondrial fragmentation and predominantly nuclear cyclin C similar to that observed in wild-type fibroblasts (representative images shown in Figure 4C, quantified in Figure 4D). These results confirmed that the aberrant cytoplasmic cyclin C and mitochondrial fragmentation was a result of the *MED13L*^{*fs*} frameshift allele and not due to a secondary mutation. Attempts to measure mitochondrial activity in the 4-1-2 or 5-1-2 corrected cell pools were confounded by reduced growth kinetics of these mortal cell lines due to senescence. Therefore, the extent to which mitochondrial function can be restored by inhibiting aberrant cyclin C-dependent fission needs further study (see Discussion).

DISCUSSION

Typical of spectrum disorders, patients with *MED13L* syndrome present with different subsets of afflictions that vary in their severity. However, the underlying cause(s) of the individual phenotypes, as well as their differences in intensity, is unknown. This study reports that *MED13L*^{+/*S1497F/fs*} patient fibroblasts exhibit reduced mitochondrial function in both fibroblasts and skeletal muscle. Mitochondrial dysfunction is at the heart of many disorders (Srivastava, 2017) including neuronal development/function (Nunnari and Suomalainen, 2012) and muscle strength (Chan, 2020; Zane et al., 2017). The proper balance between mitochondrial fission/fusion (Scheibye-Knudsen et al., 2015), and the continued supply of nuclear-encoded proteins (Jazwinski, 2013), is required for normal mitochondrial function. Importantly, loss of fusion activity through mutating the mitofusions Mfn1 and Mfn2 results in a similar response (Chen et al., 2010). With continuously fragmented mitochondria, there is a reduction in mtDNA content as well as overall activity. The underlying mechanism for this observation is not completely understood. However, defects in the distribution of mtDNA replication machinery have been observed in these fragmented organelles (Silva Ramos et al., 2019). Our findings phenocopy the fusion defective cells arguing that cyclin C-induced fragmentation is at least partially responsible for mitochondrial dysfunction observed in *MED13L*^{+/*fs*} cells. For example, in wild-type cells, the intact CKM sequesters cyclin C in the nucleus both stimulating the

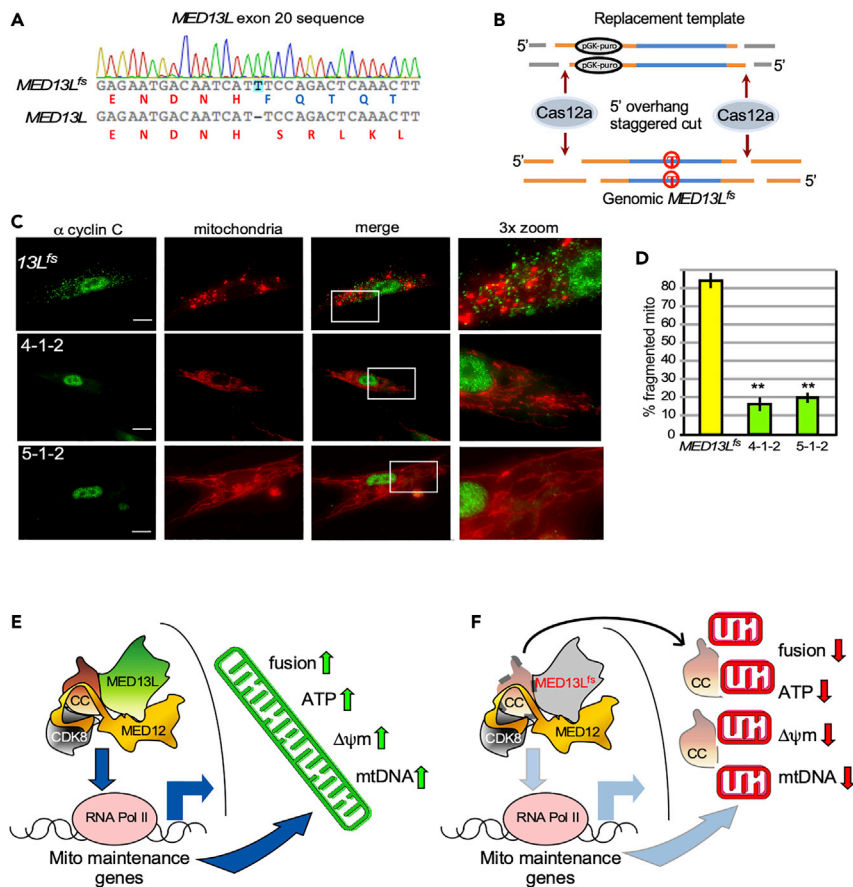


Figure 4. Correcting the *MED13L^{fs}* mutation using iCAP genome editing restores mitochondrial fusion and cyclin C nuclear localization

(A) Nucleotide sequence of *MED13L^{fs}* allele with the extra thymidine and aberrant protein sequence indicated.
 (B) iCAP strategy to introduce *MED13L* correction replacement template.
 (C) Representative images displaying cyclin C localization and mitochondrial morphology for the 4-1-2 and 5-1-2 corrected cell pools. Bar = 20 μM.
 (D) Percent of the population displaying fragmented mitochondria are quantified in the indicated cell lines (n = 3). SEM is shown, **, p < 0.01.
 (E) In normal cells, the CKM supports mitochondrial health by stimulating transcription of mitochondrial maintenance genes (MMG) and retaining cyclin C in the nucleus resulting in increased mitochondrial fusion, ATP production, stabilized mitochondrial membranes, and enhanced mtDNA integrity.
 (F) *MED13L^{fs}* mutation allows partial cyclin C nuclear release resulting in reduced MMG transcription and constitutive fragmentation leading to mitochondrial dysfunction.

transcription of nuclear encoded mitochondrial genes and preventing continuous mitochondrial fission (Figure 4E). The *MED13L^{fs}* allele allows aberrant cyclin C nuclear release that diminishes both the morphology and transcriptional arms of the mitochondrial maintenance system (Figure 4F). Finally, we demonstrated that *MED13L^{+/fs}* cells exhibit elevated endogenous ROS levels and that these cells are hypersensitivity to H₂O₂. We have previously demonstrated that forced cyclin C relocalization to the mitochondria enhances cell sensitivity to oxidative stress-induced cell death in cancer cells (Jezek et al., 2019a). In addition, neurons and muscle can be highly sensitive to elevated oxidative stress (Cheung et al., 2007; Choi et al., 2016; Kirkland et al., 2007; Reddy et al., 2011; Santos and Cardoso, 2012). Taken together, our findings provide a potential explanation underlying at least a subset of the symptoms associated with *MED13L* syndrome.

MED13/MED13L is not unique in that mutations in almost all CKM components are associated with similar developmental syndromes (reviewed in (Poot, 2020)). For example, *MED13* mutations cause heart defects

and ID (Minerath et al., 2019; Snijders Blok et al., 2018). Similarly, haplo-insufficient *MED12L* or *MED12* mutations are also associated with ID, speech impairment, and facial dysmorphism (Caro-Llopis et al., 2016; Nizon et al., 2019; Srivastava et al., 2019). Finally, several patients presenting with hypotonia, autism-like spectrum disorders, and congenital heart abnormalities were found to harbor *CDK8* (Calpena et al., 2019; Uehara et al., 2020) or *CDK19* (Chung et al., 2020; Zarate et al., 2021) mutations. Taken together, these syndromes present with overlapping disorders and have been placed into a general category of transcriptomopathies (Caro-Llopis et al., 2016; Yuan et al., 2015). The lone exception to this pattern is *CCNC*, which has not been associated with any syndromic disorders. This would not be expected if transcriptional defects were the only driving force behind these syndromes. This is especially true for *CCNC* as a paralog has not been identified unlike the other CKM components. One simple explanation is that the *CCNC* locus is resistant to mutagenesis. Another possibility is that mutations in other CKM components also require cyclin C to express their pathology. In this model, a combination of transcription mis-regulation and aberrant cytoplasmic cyclin C localization are required for expression of this disorder. Currently, we do not know if cyclin C subcellular localization is altered in these different patients, but the possibility is supported by the multiple contacts cyclin C makes with the other CKM components (Li et al., 2021). Mutating any component could impact CKM integrity and stimulate cyclin C nuclear release. Consistent with these results, a *Cnc* mutation that disrupted its interaction with Med13 or Med13L resulted in aberrant cytoplasmic localization, increased mitochondrial fission, and dysfunction in developing mouse cardiac tissue (Ponce et al., 2020). Elaborating cyclin C subcellular localization in patients with differing CKM mutations would provide insight into this question.

Correcting the *MED13L*^{fs} mutation or prohibiting cyclin C-to-mitochondrial transport resulted in rapid restoration of mitochondrial tubules. Although an indication that mitochondrial function was also returning, the activity remained well below control values. Unfortunately, these experiments were cut short when the corrected mortal *MED13L*^{+/fs} cell line senesced. However, these results beg the question of whether mitochondrial function can be restored by simply preventing cyclin C nuclear exit. The reduction in mtDNA copy number in *MED13L*^{+/fs} cells is well below the normal range of hundreds to thousands depending on the cell type. There are a few examples in which low mtDNA copy number is routinely observed. For example, sperm contains ~100 mtDNA copies and reducing this number to only a third does not significantly impede sperm cell function (Wai et al., 2010). Therefore, although the overall copy number is reduced, the range is higher than that of mitochondriopathies such as Kearns-Sayre syndrome or certain cancers (Bai and Wong, 2005; Lee et al., 2010) that exhibit more severe copy number changes. Taken together, these observations raise the possibility that mitochondrial function can be restored at least to some extent in *MED13L* syndrome cells. To what extent mitochondrial function returns and the time frame required remains an open question that will require more study.

Limitations of the study

The most important caveat to these conclusions is that only one *MED13L* syndrome cell line was examined. Concerted effort was made to secure another cell line to test but they were unsuccessful. Only through analysis of additional *MED13L* syndrome, as well as cell lines harboring mutations in other CKM components, will the generality of the findings described here be ascertained. Second, the use of mortal cell lines placed constraints on our analysis of the iCAP-corrected derivatives. The concern with immortalizing these corrected cell lines was the potential impact this would have on metabolic activity. However, in the absence of a pool of patient samples, a *MED13L* mutant-immortalized cell platform may be required to address questions concerning the rate and extent at which mitochondrial function can be restored by correcting the mutation or through pharmacological inhibition of cyclin C-dependent mitochondrial fission.

STAR★METHODS

Detailed methods are provided in the online version of this paper and include the following:

- KEY RESOURCES TABLE
- RESOURCE AVAILABILITY
 - Lead contact
 - Materials availability
 - Data and code availability
- EXPERIMENTAL MODEL AND SUBJECT DETAILS
- METHOD DETAILS

- Cell culture
- Metabolic flux analysis
- Western blot analysis
- Cyclin C immunofluorescence and mitochondrial fragmentation assay
- Mitochondrial functional assays
- Cell death assays
- *In situ* cut-and-paste (iCAP) CRISPR correction of *MED13L*^{S1497 F/fs}
- **QUANTIFICATION AND STATISTICAL ANALYSIS**

SUPPLEMENTAL INFORMATION

Supplemental information can be found online at <https://doi.org/10.1016/j.isci.2022.103823>.

ACKNOWLEDGMENTS

We thank Erin Seifert and the MitoCircle facility (Thomas Jefferson University, Philadelphia USA) for assistance in the Seahorse analysis. We thank Katrina Cooper and Vidyaramanan Ganesan for helpful comments on manuscript preparation. We thank Stephen Willis for assistance in CS mRNA determinations. This work was supported by a grant from the National Institutes of Health (GM113052) and the New Jersey Health Foundation to R. S.

AUTHOR CONTRIBUTIONS

K-T.C., J.J., and A.N.C. conducted experiments, prepared figures, and edited the manuscript. Z.A.K. analyzed LDHA levels. K.K. and P.J. performed CRISPR correction experiments. H-O.L. and W.D.K performed Seahorse experiments. R.S. and P.M.vH. conceived the experiments. R.S. wrote the manuscript and prepared figures.

DECLARATION OF INTERESTS

The authors declare no competing interests in this study.

Received: June 15, 2021

Revised: November 2, 2021

Accepted: January 21, 2022

Published: February 18, 2022

REFERENCES

- Adegbola, A., Musante, L., Callewaert, B., Maciel, P., Hu, H., Isidor, B., Picker-Minh, S., Le Caignec, C., Delle Chiaie, B., Vanakker, O., et al. (2015). Redefining the MED13L syndrome. *Eur. J. Hum. Genet.* 23, 1308–1317. <https://doi.org/10.1038/ejhg.2015.26>.
- Asadollahi, R., Zweier, M., Gogoll, L., Schiffmann, R., Sticht, H., Steindl, K., and Rauch, A. (2017). Genotype-phenotype evaluation of MED13L defects in the light of a novel truncating and a recurrent missense mutation. *Eur. J. Med. Genet.* 60, 451–464. <https://doi.org/10.1016/j.ejmg.2017.06.004>.
- Bai, R.K., and Wong, L.J. (2005). Simultaneous detection and quantification of mitochondrial DNA deletion(s), depletion, and over-replication in patients with mitochondrial disease. *J. Mol. Diagn.* 7, 613–622. [https://doi.org/10.1016/S1525-1578\(10\)60595-8](https://doi.org/10.1016/S1525-1578(10)60595-8).
- Bourbon, H.M. (2008). Comparative genomics supports a deep evolutionary origin for the large, four-module transcriptional mediator complex. *Nucleic Acids Res.* 36, 3993–4008. <https://doi.org/10.1093/nar/gkn349>.
- Calabrese, V., Lodi, R., Tonon, C., D'Agata, V., Sapienza, M., Scapagnini, G., Mangiameli, A., Pennisi, G., Stella, A.M., and Butterfield, D.A. (2005). Oxidative stress, mitochondrial dysfunction and cellular stress response in Friedreich's ataxia. *J. Neurol. Sci.* 233, 145–162. <https://doi.org/10.1016/j.jns.2005.03.012>.
- Calpena, E., Hervieu, A., Kaserer, T., Swagemakers, S.M.A., Goos, J.A.C., Popoola, O., Ortiz-Ruiz, M.J., Barbaro-Dieber, T., Bownass, L., Brilstra, E.H., et al. (2019). De novo missense substitutions in the gene encoding CDK8, a regulator of the mediator complex, cause a syndromic developmental disorder. *Am. J. Hum. Genet.* 104, 709–720. <https://doi.org/10.1016/j.ajhg.2019.02.006>.
- Caro-Llopis, A., Rosello, M., Orellana, C., Oltra, S., Monfort, S., Mayo, S., and Martinez, F. (2016). De novo mutations in genes of mediator complex causing syndromic intellectual disability: mediatoropathy or transcriptomopathy? *Pediatr. Res.* 80, 809–815. <https://doi.org/10.1038/pr.2016.162>.
- Chan, D.C. (2020). Mitochondrial dynamics and its involvement in disease. *Annu. Rev. Pathol.* 15, 235–259. <https://doi.org/10.1146/annurev-pathmechdis-012419-032711>.
- Chen, H., Detmer, S.A., Ewald, A.J., Griffin, E.E., Fraser, S.E., and Chan, D.C. (2003). Mitofusins Mfn1 and Mfn2 coordinately regulate mitochondrial fusion and are essential for embryonic development. *J. Cell Biol.* 160, 189–200.
- Chen, H., Vermulst, M., Wang, Y.E., Chomyn, A., Prolla, T.A., McCaffery, J.M., and Chan, D.C. (2010). Mitochondrial fusion is required for mtDNA stability in skeletal muscle and tolerance of mtDNA mutations. *Cell* 141, 280–289. <https://doi.org/10.1016/j.cell.2010.02.026>.
- Chen, X.J. (2013). Mechanism of homologous recombination and implications for aging-related deletions in mitochondrial DNA. *Microbiol. Mol. Biol. Rev.* 77, 476–496. <https://doi.org/10.1128/MMBR.00007-13>.
- Chen, X.J., and Butow, R.A. (2005). The organization and inheritance of the mitochondrial genome. *Nat. Rev. Genet.* 6, 815–825. <https://doi.org/10.1038/nrg1708>.

- Cheung, E.C., McBride, H.M., and Slack, R.S. (2007). Mitochondrial dynamics in the regulation of neuronal cell death. *Apoptosis* 12, 979–992. <https://doi.org/10.1007/s10495-007-0745-5>.
- Choi, M.H., Ow, J.R., Yang, N.D., and Taneja, R. (2016). Oxidative stress-mediated skeletal muscle degeneration: molecules, mechanisms, and therapies. *Oxid Med. Cell Longev.* 2016, 6842568. <https://doi.org/10.1155/2016/6842568>.
- Chung, H.L., Mao, X., Wang, H., Park, Y.J., Marcogliese, P.C., Rosenfeld, J.A., Burrage, L.C., Liu, P., Murdock, D.R., Yamamoto, S., et al. (2020). De novo variants in CDK19 are associated with a syndrome involving intellectual disability and epileptic encephalopathy. *Am. J. Hum. Genet.* 106, 717–725. <https://doi.org/10.1016/j.ajhg.2020.04.001>.
- Cooper, K.F., Khakhina, S., Kim, S.K., and Strich, R. (2014). Stress-induced nuclear-to-cytoplasmic translocation of cyclin C promotes mitochondrial fission in yeast. *Dev. Cell* 28, 161–173. <https://doi.org/10.1016/j.devcel.2013.12.009>.
- Davis, M.A., Larimore, E.A., Fissel, B.M., Swanger, J., Taatjes, D.J., and Clurman, B.E. (2013). The SCF-Fbw7 ubiquitin ligase degrades MED13 and MED13L and regulates CDK8 module association with Mediator. *Genes Dev.* 27, 151–156. <https://doi.org/10.1101/gad.207720.112>.
- Deciphering Developmental Disorders Study (2015). Large-scale discovery of novel genetic causes of developmental disorders. *Nature* 519, 223–228. <https://doi.org/10.1038/nature14135>.
- Diaz, F., and Moraes, C.T. (2008). Mitochondrial biogenesis and turnover. *Cell Calcium* 44, 24–35. <https://doi.org/10.1016/j.ceca.2007.12.004>.
- Ganesan, V., Willis, S.D., Chang, K.T., Beluch, S., Cooper, K.F., and Strich, R. (2019). Cyclin C directly stimulates Drp1 GTP affinity to mediate stress-induced mitochondrial hyperfission. *Mol. Biol. Cell* 30, 302–311. <https://doi.org/10.1091/mbc.E18-07-0463>.
- Hoepfner, S., Baumli, S., and Cramer, P. (2005). Structure of the mediator subunit cyclin C and its implications for CDK8 function. *J. Mol. Biol.* 350, 833–842. <https://doi.org/10.1016/j.jmb.2005.05.041>.
- Hori, A., Yoshida, M., and Ling, F. (2011). Mitochondrial fusion increases the mitochondrial DNA copy number in budding yeast. *Genes Cells* 16, 527–544. <https://doi.org/10.1111/j.1365-2443.2011.01504.x>.
- Hu, Y., Lu, W., Chen, G., Wang, P., Chen, Z., Zhou, Y., Ogasawara, M., Trachootham, D., Feng, L., Pelicano, H., et al. (2012). K-ras(G12V) transformation leads to mitochondrial dysfunction and a metabolic switch from oxidative phosphorylation to glycolysis. *Cell Res.* 22, 399–412. <https://doi.org/10.1038/cr.2011.145>.
- Hung, C.H., Cheng, S.S., Cheung, Y.T., Wuwongse, S., Zhang, N.Q., Ho, Y.S., Lee, S.M., and Chang, R.C. (2018). A reciprocal relationship between reactive oxygen species and mitochondrial dynamics in neurodegeneration. *Redox Biol.* 14, 7–19. <https://doi.org/10.1016/j.redox.2017.08.010>.
- Jazwinski, S.M. (2013). The retrograde response: when mitochondrial quality control is not enough. *Biochim. Biophys. Acta* 1833, 400–409. <https://doi.org/10.1016/j.bbamcr.2012.02.010>.
- Jezek, J., Chang, K.T., Joshi, A.M., and Strich, R. (2019a). Mitochondrial translocation of cyclin C stimulates intrinsic apoptosis through Bax recruitment. *EMBO Rep.* 20, e47425. <https://doi.org/10.15252/embr.201847425>.
- Jezek, J., Smethurst, D.G.J., Stieg, D.C., Kiss, Z.A.C., Hanley, S.E., Ganesan, V., Chang, K.T., Cooper, K.F., and Strich, R. (2019b). Cyclin C: the story of a non-cycling cyclin. *Biology (Basel)* 8. <https://doi.org/10.3390/biology8010003>.
- Khakhina, S., Cooper, K.F., and Strich, R. (2014). Med13p prevents mitochondrial fission and programmed cell death in yeast through nuclear retention of cyclin C. *Mol. Biol. Cell* 25, 2807–2816. <https://doi.org/10.1091/mbc.E14-05-0953>.
- Kirkland, R.A., Saavedra, G.M., and Franklin, J.L. (2007). Rapid activation of antioxidant defenses by nerve growth factor suppresses reactive oxygen species during neuronal apoptosis: evidence for a role in cytochrome c redistribution. *J. Neurosci.* 27, 11315–11326. <https://doi.org/10.1523/JNEUROSCI.3590-07.2007>.
- Lee, H.C., Chang, C.M., and Chi, C.W. (2010). Somatic mutations of mitochondrial DNA in aging and cancer progression. *Ageing Res. Rev.* 9, S47–S58. <https://doi.org/10.1016/j.arr.2010.08.009>.
- Li, J., O, W., Li, W., Jiang, Z.G., and Ghanbari, H.A. (2013). Oxidative stress and neurodegenerative disorders. *Int. J. Mol. Sci.* 14, 24438–24475. <https://doi.org/10.3390/ijms141224438>.
- Li, N., Fassel, A., Chick, J., Inuzuka, H., Li, X., Mansour, M.R., Liu, L., Wang, H., King, B., Shaik, S., et al. (2014). Cyclin C is a haploinsufficient tumour suppressor. *Nat. Cell Biol.* 16, 1080–1091. <https://doi.org/10.1038/ncb3046>.
- Li, R., Beebe, T., Cui, J., Rouhanizadeh, M., Ai, L., Wang, P., Gundersen, M., Takabe, W., and Hsiai, T.K. (2009). Pulsatile shear stress increased mitochondrial membrane potential: implication of Mn-SOD. *Biochem. Biophys. Res. Commun.* 388, 406–412. <https://doi.org/10.1016/j.bbrc.2009.08.022>.
- Li, Y.C., Chao, T.C., Kim, H.J., Cholko, T., Chen, S.F., Li, G., Snyder, L., Nakanishi, K., Chang, C.E., Murakami, K., et al. (2021). Structure and noncanonical Cdk8 activation mechanism within an Argonaute-containing Mediator kinase module. *Sci. Adv.* 7, eabd4484. <https://doi.org/10.1126/sciadv.abd4484>.
- Minerath, R.A., Dewey, C.M., Hall, D.D., and Grueter, C.E. (2019). Regulation of cardiac transcription by thyroid hormone and Med13. *J. Mol. Cell Cardiol.* 129, 27–38. <https://doi.org/10.1016/j.yjmcc.2019.01.007>.
- Nicholls, D.G. (2006). Simultaneous monitoring of ionophore- and inhibitor-mediated plasma and mitochondrial membrane potential changes in cultured neurons. *J. Biol. Chem.* 281, 14864–14874. <https://doi.org/10.1074/jbc.M510916200>.
- Nizon, M., Laugel, V., Flanigan, K.M., Pastore, M., Waldrop, M.A., Rosenfeld, J.A., Marom, R., Xiao, R., Gerard, A., Pichon, O., et al. (2019). Variants in MED12L, encoding a subunit of the mediator kinase module, are responsible for intellectual disability associated with transcriptional defect. *Genet. Med.* 21, 2713–2722. <https://doi.org/10.1038/s41436-019-0557-3>.
- Nunnari, J., and Suomalainen, A. (2012). Mitochondria: in sickness and in health. *Cell* 148, 1145–1159. <https://doi.org/10.1016/j.cell.2012.02.035>.
- Phillips, N.R., Sprouse, M.L., and Roby, R.K. (2014). Simultaneous quantification of mitochondrial DNA copy number and deletion ratio: a multiplex real-time PCR assay. *Sci. Rep.* 4, 3887. <https://doi.org/10.1038/srep03887>.
- Ponce, J.M., Coen, G., Spittler, K.M., Dragisic, N., Martins, I., Hinton, A., Jr., Mungai, M., Tadinada, S.M., Zhang, H., Oudiz, G.Y., et al. (2020). Stress-induced cyclin C translocation regulates cardiac mitochondrial dynamics. *J. Am. Heart Assoc.* 9, e014366. <https://doi.org/10.1161/JAHA.119.014366>.
- Poot, M. (2020). Mutations in mediator complex genes CDK8, MED12, MED13, and MED13L mediate overlapping developmental syndromes. *Mol. Syndromol.* 10, 239–242. <https://doi.org/10.1159/000502346>.
- Reddy, T.P., Manczak, M., Calkins, M.J., Mao, P., Reddy, A.P., Shirendeb, U., Park, B., and Reddy, P.H. (2011). Toxicity of neurons treated with herbicides and neuroprotection by mitochondria-targeted antioxidant SS31. *Int. J. Environ. Res. Public Health* 8, 203–221. <https://doi.org/10.3390/ijerph8010203>.
- Santos, D., and Cardoso, S.M. (2012). Mitochondrial dynamics and neuronal fate in Parkinson's disease. *Mitochondrion* 12, 428–437. <https://doi.org/10.1016/j.mito.2012.05.002>.
- Satoh, M., and Kuroiwa, T. (1991). Organization of multiple nucleoids and DNA molecules in mitochondria of a human cell. *Exp. Cell Res.* 196, 137–140. [https://doi.org/10.1016/0014-4827\(91\)90467-9](https://doi.org/10.1016/0014-4827(91)90467-9).
- Scheibye-Knudsen, M., Fang, E.F., Croteau, D.L., Wilson, D.M., 3rd, and Bohr, V.A. (2015). Protecting the mitochondrial powerhouse. *Trends Cell Biol.* 25, 158–170. <https://doi.org/10.1016/j.tcb.2014.11.002>.
- Silva Ramos, E., Motori, E., Bruser, C., Kuhl, I., Yeroslaviz, A., Ruzzenente, B., Kauppila, J.H.K., Busch, J.D., Hultenby, K., Habermann, B.H., et al. (2019). Mitochondrial fusion is required for regulation of mitochondrial DNA replication. *PLoS Genet.* 15, e1008085. <https://doi.org/10.1371/journal.pgen.1008085>.
- Snijders Blok, L., Hiatt, S.M., Bowling, K.M., Prokop, J.W., Engel, K.L., Cochran, J.N., Bebin, E.M., Bijlsma, E.K., Ruivenkamp, C.A.L., Terhal, P., et al. (2018). De novo mutations in MED13, a component of the Mediator complex, are associated with a novel neurodevelopmental disorder. *Hum. Genet.* 137, 375–388. <https://doi.org/10.1007/s00439-018-1887-y>.
- Srivastava, S. (2017). The mitochondrial basis of aging and age-related disorders. *Genes (Basel)* 8, 398. <https://doi.org/10.3390/genes8120398>.
- Srivastava, S., Niranjan, T., May, M.M., Tarpey, P., Allen, W., Hackett, A., Jouk, P.S., Raymond, L., Briault, S., Skinner, C., et al. (2019).

Dysregulations of sonic hedgehog signaling in MED12-related X-linked intellectual disability disorders. *Mol. Genet. Genomic Med.* 7, e00569. <https://doi.org/10.1002/mgg3.569>.

Stieg, D.C., Chang, K.T., Cooper, K.F., and Strich, R. (2019). Cyclin C regulated oxidative stress responsive transcriptome in *Mus musculus* embryonic fibroblasts. *G3 (Bethesda)* 9, 1901–1908. <https://doi.org/10.1534/g3.119.400077>.

Stieg, D.C., Willis, S.D., Ganesan, V., Ong, K.L., Scuzo, J., Song, M., Grose, J., Strich, R., and Cooper, K.F. (2018). A complex molecular switch directs stress-induced cyclin C nuclear release through SCF(Grr1)-mediated degradation of Med13. *Mol. Biol. Cell* 29, 363–375. <https://doi.org/10.1091/mbc.E17-08-0493>.

Strom, E., Sathe, S., Komarov, P.G., Chernova, O.B., Pavlovska, I., Shyshynova, I., Bosykh, D.A., Burdelya, L.G., Macklis, R.M., Skaliter, R., et al. (2006). Small-molecule inhibitor of p53 binding to mitochondria protects mice from gamma radiation. *Nat. Chem. Biol.* 2, 474–479.

Torring, P.M., Larsen, M.J., Brasch-Andersen, C., Krogh, L.N., Kibaek, M., Laulund, L., Illum, N., Dunkhase-Heinl, U., Wiesener, A., Popp, B., et al. (2019). Is MED13L-related intellectual disability a recognizable syndrome? *Eur. J. Med. Genet.* 62, 129–136. <https://doi.org/10.1016/j.ejmg.2018.06.014>.

Uehara, T., Abe, K., Oginuma, M., Ishitani, S., Yoshihashi, H., Okamoto, N., Takenouchi, T., Kosaki, K., and Ishitani, T. (2020). Pathogenesis of CDK8-associated disorder: two patients with novel CDK8 variants and in vitro and in vivo functional analyses of the variants. *Sci. Rep.* 10, 17575. <https://doi.org/10.1038/s41598-020-74642-4>.

van Haelst, M.M., Monroe, G.R., Duran, K., van Binsbergen, E., Breur, J.M., Giltay, J.C., and van Haaften, G. (2015). Further confirmation of the MED13L haploinsufficiency syndrome. *Eur. J. Hum. Genet.* 23, 135–138. <https://doi.org/10.1038/ejhg.2014.69>.

Vander Heiden, M.G., Cantley, L.C., and Thompson, C.B. (2009). Understanding the Warburg effect: the metabolic requirements of cell proliferation. *Science* 324, 1029–1033. <https://doi.org/10.1126/science.1160809>.

Wai, T., Ao, A., Zhang, X., Cyr, D., Dufort, D., and Shoubridge, E.A. (2010). The role of mitochondrial DNA copy number in mammalian fertility. *Biol. Reprod.* 83, 52–62. <https://doi.org/10.1095/biolreprod.109.080887>.

Wang, K., Yan, R., Cooper, K.F., and Strich, R. (2015). Cyclin C mediates stress-induced mitochondrial fission and apoptosis. *Mol. Biol. Cell* 26, 1030–1043. <https://doi.org/10.1091/mbc.E14-08-1315>.

Youngman, M.J., Hobbs, A.E., Burgess, S.M., Srinivasan, M., and Jensen, R.E. (2004). Mmm2p, a mitochondrial outer membrane protein required for yeast mitochondrial shape and maintenance of mtDNA nucleoids. *J. Cell Biol.* 164, 677–688. <https://doi.org/10.1083/jcb.200308012>.

Yuan, B., Pehlivan, D., Karaca, E., Patel, N., Charng, W.L., Gambin, T., Gonzaga-Jauregui, C., Sutton, V.R., Yesil, G., Bozdogan, S.T., et al. (2015). Global transcriptional disturbances underlie Cornelia de Lange syndrome and related phenotypes. *J. Clin. Invest.* 125, 636–651. <https://doi.org/10.1172/JCI77435>.

Zane, A.C., Reiter, D.A., Shardell, M., Cameron, D., Simonsick, E.M., Fishbein, K.W., Studenski, S.A., Spencer, R.G., and Ferrucci, L. (2017). Muscle strength mediates the relationship between mitochondrial energetics and walking performance. *Aging Cell* 16, 461–468. <https://doi.org/10.1111/acer.12568>.

Zarate, Y.A., Uehara, T., Abe, K., Oginuma, M., Harako, S., Ishitani, S., Lehesjoki, A.E., Bierhals, T., Kloth, K., Ehmeke, N., et al. (2021). CDK19-related disorder results from both loss-of-function and gain-of-function de novo missense variants. *Genet. Med.* 23, 1050–1057. <https://doi.org/10.1038/s41436-020-01091-9>.

STAR★METHODS

KEY RESOURCES TABLE

REAGENT or RESOURCE	SOURCE	IDENTIFIER
Antibodies		
cyclin C	ThermoScientific	PA5-16227; RRID:AB_10982613
Alexa Fluor 488-conjugated secondary antibody	ThermoScientific	A11008; RRID:AB_143165
alkaline phosphatase-conjugated rabbit secondary antibody	Abcam	ab97061; RRID:AB_10680575
LDHA	Santa Cruz Biotechnology	SC-137243; RRID:AB_2137192
β-actin	Merck	A1978; RRID:AB_476692
dsDNA	Dev. Studies Hybridoma Bank	RRID:AB_10805293
Chemicals, peptides, and recombinant proteins		
H ₂ O ₂	ACS Chemical	UN2014
Pifithrin μ	TGI Chemica	P2048
carbonyl cyanide <i>p</i> -trifluoromethoxyphenylhydrazone	Cayman Chemical	15218
Oligomycin	Sigma	49455
Rotenone	Sigma	R8875
Antimycin A	Sigma	R8875
MitoTempo	Sigma	SML0737
Actinomycin D	Cayman Chemical	11421
Tetramethylrhodamine (TMRM)	Invitrogen	I34361
Critical commercial assays		
Annexin V Cell Death Assay	BD Biosciences	556419
Bradford Protein	Bio-Rad	5000001
Experimental models: Cell lines		
MED13L ^{S1497F/+} human dermal fibroblast	Center for Molecular Medicine UMC Utrecht Netherlands	N/A
MED13L ^{+/+} human dermal fibroblast corrected allele	This study	N/A
WI-38	ATCC	CCL-75
Experimental models: Organisms/strains		
XL-1 Blue <i>Escherichia coli</i>	Agilent	200249
Oligonucleotides		
MED13L exon 20, Forward AGCCTAGTCCAAGTTTAGAGAG	This study	N/A
MED13L exon 20, Reverse AAACTGCCAGAACACCAAAGTGG	This study	N/A
M13 Sequencing Primer Forward TGTAACGACGGCCAGT	This study	N/A
M13 Sequencing Primer, Reverse CAGGAAACAGCTATGAC	This study	N/A
MED13L intron19-20, Forward CGATCAGCATACTCACTGCTTCAG	This study	N/A
MED13L intron19-20, Reverse GTCTCCTTCAGACTGATTCCATG	This study	N/A
mtMinArc Forward CTAATAGCCACACGTTCCC	mt 16,528 – 16,548	(Phillips et al., 2014)

(Continued on next page)

Continued

REAGENT or RESOURCE	SOURCE	IDENTIFIER
mtMinArc Reverse AGAGCTCCCGTGAGTGGTTA	<i>mt</i> 23-42	(Phillips et al., 2014)
Fβ2M Forward GCTGGGTAGCTCTAAACAATGTATTCA	<i>Chr15</i> 15,798,932 – 15,798,95	(Phillips et al., 2014)
Fβ2M Reverse CCATGTACTAACAAAT GTCTAAAATGGT	<i>Chr15</i> 15,798,999 – 15,799,02	(Phillips et al., 2014)
Recombinant DNA		
pGL3-U6-sgRNA-PGK-puromycin	Addgene	51133
pTE4398	Addgene	74042
pX330S-2	Addgene	58778

RESOURCE AVAILABILITY

Lead contact

Further information and requests for resources and reagents should be directed to, and will be fulfilled by, the lead contact, Randy Strich (streichra@rowan.edu)

Materials availability

The *MED13L*^{+/*fs*} mutant and corrected cell lines described in this study will be made available upon request and proper consent.

Data and code availability

Data generated in this study will be provided upon request. The *Ccnc*^{-/-} transcriptome dataset has been deposited previously (GEO accession is GSE126450). Methods to interpret the data are detailed in the STAR method section of this manuscript. This paper does not report original code. Any additional information required to reanalyze the data reported in this paper is available from the lead contact upon request.

EXPERIMENTAL MODEL AND SUBJECT DETAILS

Dermal fibroblasts from a *MED13L* syndrome 6 year old male patient were obtained from a skin biopsy, cultured and stored. Cells were obtained with written consent of the patient's representative. WI-38 cells were obtained from the ATCC. The human fibroblast cell line (*MED13L*^{S1497 F/*fs*}) was obtained following informed consent with the identification of the donor blinded from the participants in this study. WI-38 embryonic lung fibroblasts were obtained from the ATCC.

METHOD DETAILS

Cell culture

The cells were cultured in DMEM, 10% fetal bovine serum (FBS) and 1% penicillin/streptomycin (PS). Cells were passaged by brief treatment (2 min) with trypsin/EDTA with gentle tapping of the dish. Collected cells were counted and replated to provide approximately 20% confluency for WI-38, 25% for *MED13L*^{*fs*} cells. All incubations were conducted in this medium except for H₂O₂ treatment, which was performed in FBS- and PS-free medium. Pifithrin μ (PFT) was dissolved in DMSO and added to cells at a final concentration of 1 μM for the times indicated. The cell culture medium was changed daily and additional PFT was daily for multi-day experiments.

Metabolic flux analysis

The oxygen consumption rate (OCR) and extracellular acidification rate (ECAR) were measured by the Seahorse XF96 Analyzer (Agilent Technologies, Santa Clara, CA). WI-38 or *MED13L*^{+/*fs*} cells were grown in XF96 microplates then incubated in a 37°C, non-CO₂ incubator for one hour with the designated medium. The assay medium for the mitochondrial stress assay was Seahorse XF DMEM medium, pH 7.4 containing 10 mM glucose, 2 mM glutamine and 1 mM pyruvate. The assay medium for glycolytic stress assays was Seahorse XF DMEM medium, pH 7.4 containing 2 mM glutamine. Metabolic data were normalized to cell number after the assay. Each experiment was conducted in 14 separate wells with the

results averaged \pm standard error of the mean (SEM). Statistical significance was determined by the Students T test.

Western blot analysis

Whole-cell extracts (WCE) were prepared from cells harvested following trypsin-EDTA treatment. The cells were washed with 4 °C PBS and incubated with CHAPS lysis buffer (CLB, 150 mM NaCl, 10 mM HEPES, 1% CHAPS, pH 7.4) containing 1% protease inhibitor cocktail (PIC) for 30 min at 4 °C. WCEs were centrifuged at 14,000 \times g for 15 min at 4 °C to separate soluble proteins from cell debris. Soluble protein concentrations were determined by Bradford assay (Bio-Rad, Hercules, CA). Western blots were visualized and quantified by phosphorimaging (iBright 1500, Thermo Scientific) using alkaline phosphatase-conjugated rabbit secondary antibody and CDP-Star as substrate. Blots were initially probed with LDHA antibodies then stripped and re-probed with β -actin for a loading control.

Cyclin C immunofluorescence and mitochondrial fragmentation assay

Cells were cultured on poly-L-lysine-coated coverslips for 2 d, stained with 100 nM MitoTracker Red CMXRos for 30 min at 37 °C, fixed with 4% paraformaldehyde for 10 min, permeabilized with 0.2% Triton X-100 for 10 min, blocked with 2% BSA for 30 min, and incubated with 4 mg/mL cyclin C antibody at 4 °C overnight. Slides were washed in PBS and 1 mg/mL Alexa Fluor 488-conjugated secondary antibody for 1 h. Fixed cells were mounted with 4',6-diamidino-2-phenylindole (DAPI)-containing medium to stain the nuclei. Images were acquired with an Eclipse 90i microscope (Nikon, Tokyo, Japan) using the 100 \times oil objective (NA 1.25). Mitochondrial DNA immunofluorescence was accomplished as just described using α -dsDNA antibodies as primary. All images of a particular stain were collected with identical exposure times. Imaging processing was limited to adjusting exposures to permit visualization of all components in merged images. All merged images were adjusted identically. Mitochondria were scored as fragmented when cells contained >15 puncta with <10 mitochondria with a length of 10 μ m or more were considered fragmented (Wang et al., 2015). NIS-Elements software (Nikon) was used for image deconvolution and analysis.

Mitochondrial functional assays

Cells were stained with 4 μ m MitoSOX Red for 15 min at 37 °C, washed twice with FluoroBrite DMEM, and signals quantified using an Accuri C6 flow cytometer (BD Biosciences, San Jose, CA). Tetramethylrhodamine methyl ester (TMRM) staining was conducted as suggested by the manufacturer. Changes in mitochondrial membrane potential ($\Delta\Psi_m$) were calculated using TMRM fluorescence levels as described (Li et al., 2009) using the Nernst equation (Nicholls, 2006). Cells were seeded in 12 well plates and treated with or without PFT (1 μ m). For the assay, cells were treated with 80 μ m CCCP for 5 min and then treated with 200 nM TMRM at 37 °C for 30 min. Cells were harvested and then analyzed by flow cytometry (Attune NXT, ThermoFisher). To calculate membrane potential, CCCP + TMRM intensities for WI-38 and MED13L^{fs} were used as the unstimulated (or background) values. TMRM stimulated = fluorescent intensity (TMRM with or without PFT added) – background values.

Cell death assays

Cells were grown in 12-well plates (VWR, Radnor, PA) for 2 days and treated with H₂O₂ (0.4 mM for 16 h) as indicated in the text. Annexin V assays were conducted as described by the manufacturer on an Accuri C6 flow cytometer (BD Biosciences). Only Annexin V⁺ and propidium iodide (PI)⁻ cells were plotted as they were considered early apoptotic without necrotic cell contribution to the signal.

In situ cut-and-paste (iCAP) CRISPR correction of MED13L^{S1497 F/fs}

Briefly, genomic DNA extracted from frozen cell culture samples of human WI-38 and MED13L^{+/fs} fibroblasts was subjected to PCR amplification of exon 20. The fragments were subcloned into pGL3-U6-sgRNA-PGK-puromycin using XL1-Blue *E. coli* for amplification prior to DNA sequence analysis. The analysis revealed a mutation in MED13L exon 20 NM_015335.5;c.[5054dupT];[Ser1497Phe^{fs}] (Chr12(GRCh38):t.[116252045dup]). Briefly, iCAP editing was accomplished by excising the endogenous mutant exon 20 from the MED13L allele by cleavages induced by Cas9 (pX330S-2) or Cas12a/Cpf1 (pTE4398) at two gRNA target sites, one in intron 19-20 and the other in intron 20-21. Intronic sequences flanking exon 20 are identical in the wild-type and mutant MED13L alleles. Potential Cas9 or Cas12a (Cpf1) gRNA target sequences were identified using the online tool "Benchling" (<https://www.benchling.com/crispr/>, San

Francisco, CA). The mutant allele was replaced by pasting the wild-type exon 20 containing a puromycin selection marker gene placed in intron 19-20 (P.J. and R.S., personal communication). The edited isogenic fragment was pre-constructed in a DNA replacement template (dRT) *in vitro* and was excised from the dRT by CRISPR/Cas12a cleavages which also simultaneously occurred to the endogenous *MED13L* gene *in situ*.

QUANTIFICATION AND STATISTICAL ANALYSIS

The student's *t* test was applied to calculate statistical differences with *p* values < 0.05 considered significantly different. *p* values are discriminated for each experiment as described in the figure legends. Standard error of the mean (S.E.M.) is presented in each figure.